January 2012

Analyzing Breast Tumor Response To Neoadjuvant Therapy By Pk Models Of Dynamic--contrast Enhanced Mr

Matthew Lidstrom

Analyzing Breast Tumor Response to Neoadjuvant Therapy By PK Models of Dynamic-Contrast Enhanced MR

A Thesis Submitted to the

Yale University School of Medicine

In Partial Fulfillment of the Requirements for the

Degree of Doctor of Medicine

By

Matthew Scott Lidstrom

2012

Abstract

Introduction: Pharmacokinetic modeling of contrast uptake by Dynamic-Contrast Enhanced Magnetic Resonance Imaging studies has shown potential to predict the pathologic response to neoadjuvant therapy in breast cancer patients via several small studies. We will attempt to prospectively validate the performance of several previously published criteria in women undergoing neoadjuvant therapy with bevacizumab or trastuzumab.

Methods: 11 patients underwent dynamic contrast enhanced magnetic resonance imaging both before and after receiving one cycle of trastuzumab or bevacizumab neoadjuvant chemotherapy for a primary breast lesion of greater than two centimeters. By abstracting pharmacokinetic parameters (Ktrans) from each study, predictions for therapeutic response based on previously published criteria (Ah-See and Yu utilize a threshold for percentage change in median Ktrans; Padhani, a percentage change in Ktrans range) were compared with the response by pathology acquired after completion of neoadjuvant therapy.

Results: 7 patients were able to successfully complete imaging at the two requisite time points. All utilized criteria correctly identified 5/5 non-responders; the Ah-See and Padhani criteria were able to identify 1/2 positive responders; and the Yu criterion identified 0/2 positive responders.

Discussion: The efficacy of the Ah-See and Padhani criteria identify responders and non-responders equally well. Due to the Padhani criterion's susceptibility to noise, however, it is likely that Ah-See would outperform Padhani on a larger cohort.

Acknowledgements

Thanks to Dan Cornfeld, my mentor, for all his hard work and guidance. Thanks also to my wife, Shelby, for her love, support and care.

Introduction

The non-invasive qualification and quantification of neoplastic lesions poses obvious benefits to patient care. Unfortunately, while there exist imaging modalities suited to qualifying tumor characteristics, obtaining clinically relevant measures of malignancy often requires physical sampling for ex-vivo pathological evaluation in addition to any imaging. As new anti-cancer agents whose primary effect may not initially be cytolysis become increasingly common in clinical practice, the development of non-invasive staging techniques that investigate histologic or metabolic features not traditionally appreciated via anatomical imaging becomes necessary. This study will examine one such proposed imaging modality: pharmacokinetic (PK) modeling of Dynamic Contrast-Enhanced Magnetic Resonance Imaging (DCE-MRI). In particular, DCE-MRI will be used to evaluate the response of patients with breast cancer to the neoadjuvant therapy with the antiangiogenic agents bevacizumab and trastuzumab.

Clinically evaluating anti-angiogenesis agents in breast cancer: the need for DCE-MRI

Anti-angiogenesis agents like bevacizumab are recombinant humanized monocolonal antibody that blocks the effects Vascular Endothelial Growth Factor (VEGF). Bavacizumab's pharmacologic mechanism involves binding to, and thus inhibiting, the cellular receptors of VEGF. VEGF, itself, is a potent inducer of many effects thought to be important to the progression of cancer, including mitogenic and prosurvival functions on vascular endothelial cells; angiogenesis; and induction

of the formation of fenestrations in the endothelial lining of vessels [1]. To that end, initial animal studies of bevacizumab have demonstrated *in-vivo* inhibition of tumor growth in mice [2], an effect which has been replicated in humans in many different solid tumor types [3-6].

Breast cancer presents a particularly attractive target for bevacizumab because many of its histologic subtypes have been shown to over-express the VEGF receptor [7] and indeed, studies have indicated the prognostic value of VEGF expression in response to therapy [8,9]. Accordingly, three large randomized controlled trials have demonstrated that the addition of bevacizumab to selected first-line, small-molecule-based chemotherapies increases the progression-free survival of certain patients with breast cancer [10-12]. Interestingly, this benefit to progression free survival interval did not correspond with an increase in overall survival in the studies. This discordance has led to bevacizumab's disapproval for use as part of the primary chemotherapeutic regimen in breast cancer via the United States Food and Drug Administration. It should be noted, however, that these large studies were designed and conducted according to long-established and familiar criteria for measuring outcome. As will be discussed, these measurements do not directly quantify the physiologic action of agents such as bevacizumab.

There exist two classification schemes accepted by the Food and Drug Administration for the measurement and reporting of tumor response to therapy during clinical trials: the world health organization guidelines (WHO)[13] and the

more recently developed Response Evaluation Criteria in Solid Tumors (RECIST)[14]. Both WHO and RECIST guidelines define surrogate clinical endpoints such as response and progression free survival based on serial changes in tumor size. . Both utilize thresholds of percentage change of the largest-measured diameter (two-dimensional in the case of WHO, and one dimensional in the case of RECIST) to classify disease as progressive, stable, or a partial responder (note that complete response is also defined, but as the absence of apparent disease). Such schemes are less than ideal for the evaluation of anti-angiogenic agents such as bevacizumab, which are thought to be cytostatic[15] and may not result in immediate tumor shrinkage. Thus, bevacizumab's efficacy may not be well reflected in the traditional size-based endpoints incorporated into its clinical trials to date.

The need for a well-tailored, non-invasive means for detecting the activity of anti-angiogenic agents such as bevacizumab goes beyond the potential for higher quality research design. Indeed, as neoadjuvant therapy has become increasingly utilized in breast cancer [16], the determination of a given patient's pathological response early in their course of therapy is important as it bears prognostic significance and may influence outcome[17]. Interestingly, a potentially clinically relevant pathological response to bevacizumab may be detected as early as 48 hours after the initiation of therapy[18]. Therefore, while it appears to be possible to gauge a patient's response to therapy with anti-angiogenic agents, to investigate and potentially utilize them in the neoadjuvant role, one's current options for clinical assessment are less than ideal: either subject the patient to invasive pathological biopsy or rely on

established size-based biomarkers that may not strongly correlate with *in-vivo* activity.

This begs the question: if the metrics traditionally utilized to evaluate cytotoxic chemotherapeutic agents are potentially inadequate to evaluate anti-angiogenic agents, are there other more effective imaging biomarkers? One of the most promising imaging biomarkers is DCE-MRI[19]. This study will attempt to further evaluate DCE-MRI's efficacy in this role.

DCE-MRI and Pharmacokinetic Modeling

The DCE-MRI moniker encompasses a wide range of magnetic resonance imaging study designs. It has been employed to characterize lesions of many different histologic types including: breast, prostate[20], brain[21], liver[22], and cervix[23] among others. Despite the variety of pathology surveyed, each imaging study incorporates a very simple mechanism: inject an extracellular contrast agent during MR signal acquisition so that, in the completed study, disparate phases of contrast wash-in and washout can be evaluated with some sort of analysis.

In its basic implementation, DCE-MRI is commonly used as a tool for evaluating solid organ masses.. For example, the diagnosis of several common liver lesions can be made based on a lesion's appearance on images obtained at three specific time points following the administration of a CT or MRI contrast agent. Focal nodular hyperplasia enhances briskly in the arterial phase and then becomes iso-

intense/iso-dense to the liver parenchyma on delayed images. Hepatic hemangiomas display peripheral, nodular, discontinuous enhancement in the arterial phase and gradually fill with contrast at more delayed time points. Hepatocellular carcinoma enhances briskly in the artierial phase and then becomes hypo-dense/hypo-intense to the liver parenchyma on delayed images. The subjective evaluation of a lesion's enhancement characteristics over time is the simplest form of DCE-MRI.

A semi-quantitative example of DCE-MRI is used in the diagnosis of breast cancer. Early investigators evaluated contrast uptake and washout in clinically suspicious breast lesions[24]. In their analysis of signal intensity curves obtained from nine time points approximately forty-seconds apart they stratified the resulting time-intensity shape following bolus arrival into one of the three classes of form demonstrated in Figure 1: uptake, plateau, and washout. Through this, they were able to show that malignant tumors were more likely to enhance and then de-enhance (consistent with the washout curve)where-as benign lesions tended to enhance progressively (consistent with the continued uptake curve). (p<.001, sensitivity 91%, specificity 83%). Further investigations would confirm this trend in morphology[25,26], though with insufficient specificity to be useful in confidently distinguishing benign from malignant breast tissue. Nevertheless, the current standard of care in breast MRI is to obtain high spatial resolution images of the breast before contrast, during the first pass arterial phase, and then again 5-6 minutes later and analyze the resulting signal enhancement curve. This is a semi-quantitative example of DCE-MRI.

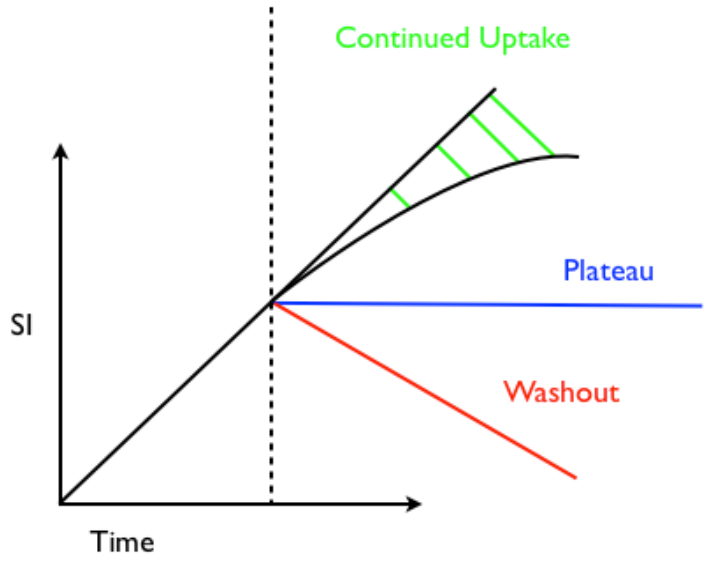

Figure1 Diagrammatic representation of the three categories of signal intensity (SI) curves noted after initial upstroke from the bolus (dashed line marks the end of this period): continued uptake, plateau, and washout.

Multiple strategies to quantify curve morphology have been proposed and vary from measuring the initial slope of the curve[27], to finding the area under the curve after some elapsed time period[28], to some of the approaches discussed in greater detail in this paper. What these methods have in common is that they attempt to capture the pharmacokinetic behavior of contrast as it diffuses into normal and pathologic tissues. For instance, one such method -- signal enhancement ratio (SER) -- is calculated by measuring the signal in a lesion at three different time points S_0, S_1, S_2 (corresponding to pre-bolus administration, estimated peak-signal during the first pass arterial phase, and after enough time has passed to reach steady state, respectively) [29]. SER is calculated as $\frac{S_1 - S_0}{S_2 - S_0}$. High SER values correspond to tumors that enhance briskly and then de-enhance. Low SER values correspond to tumors that either show low levels of initial enhancement or progressive delayed

enhancement. SER has been studied in a limited population of breast cancer patients as a predictor of resurrence following chemotherapy. Tumors with large areas of increased SER were more likely to recur following chemotherapy than tumors with low SER[30]. However, its accuracy in that study (75% correctly identified, but only 35% correctly identified before chemotherapy) leaves much to be desired if it is to be employed as tool for clinical decision making.

More rigorous attempts at qualitatively analyzing time-enhancement curves involve the use of true pharmacokinetic models. The most popular model was first described by Tofts et al and variants of this model are recommended by the National Cancer Institute in the US and the Pharmacodynamic/Pharmacokinetic Technologies Advisory Committee in the United Kingdom whenever analysis of DCE-MRI is to be used as an imaging biomarker[31]. The Tofts model is a simple two compartmental model diagrammed in Figure 2. In it, contrast is introduced into the blood plasma (compartment #1) and is either excreted by the kidneys at a concentration-dependent rate k2 or leaks across a vascular barrier into a tumor tissue (compartment #2) at a concentration-dependent rate k1. In this model, the contrast agent only has access to the extracellular space of the tumor (i.e. the contrast agent does not actually enter into cells) , so the extracellular fraction of the tumor becomes an explicit subcomponent of the tissue compartment. If v_e represents the fraction of tumor that is extracellular space then the relationship between the concentration of contrast in the tissue compartment ($c_t(t)$) and its extracellular subspace ($c_e(t)$) is

$$c_t(t) = v_e c_e(t) \qquad (1)$$

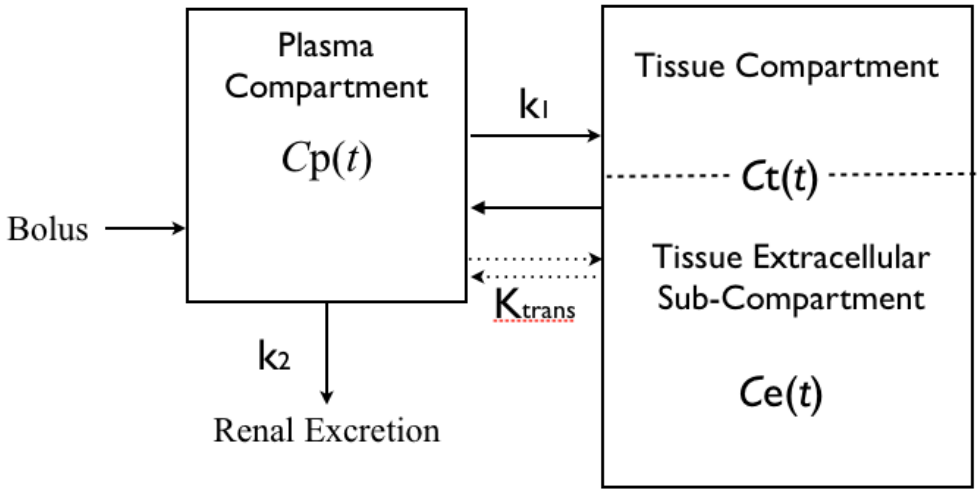

Figure 2 The Tofts Model. A two compartmental model is shown where concentration of contrast in the plasma compartment is Cp(t), and the tissue compartment is Ct(t). Note that the fraction of the tissue compartment's volume that is accessible to contrast (ve) is also diagrammed, the extracellular sub-compartment and it's concentration of contrast is given by Ce(t). k1 represents the rate constant governing concentration-dependent movement of plasma between tumor and plasma, Ktrans between the extracellular sub-compartment, and k2 the rate of renal excretion.

According to Tofts, the total amount of contrast in tissue is therefore given as $v_e V_t c_e(t)$ where V_t is the total volume of the tumor. This amount is assumed to change proportionately to the difference in contrast concentrations between the extracellular space and plasma according to the following differential equation

$$v_e V_t \frac{dc_e(t)}{dt} = PS[c_p(t) - c_e(t)] \qquad (2)$$

where S is the total surface area of the microvasculature within the tumor and P is the permeability of the tumor capillaries. By defining $K_{trans} = \frac{PS}{V_t}$ as the volume transfer coefficient (units of 1/min) and recalling equation (1), equation (2) becomes

$$\frac{dc_t(t)}{dt} = K_{trans}\left[c_p(t) - {c_t(t)}/{v_e}\right]$$

Furthermore, if we let $k_{ep} = K_{trans} / v_e$ then

$$\frac{dc_t(t)}{dt} = K_{trans} c_p(t) - k_{ep} c_t(t)$$

In this setting, K_{trans} represents the rate constant for contrast flow across the capillaries into the tumor (normalized to tumor volume), and k_{ep} represents the rate constant for contrast passage from the tumor back into the capillaries. When combined with initial conditions $c_p(0) = c_t(0) = 0$, this differential equation has an implicit solution,

$$c_t(t) = K_{trans} \int_o^t c_p(\tau) e^{-k_{ep}(t-\tau)} d\tau = c_p(t) \otimes \{K_{trans} e^{-k_{ep} t}\} \quad (3)$$

Equation (3) provides a highly useful interpretation: the concentration of contrast in tissue can be broken into two independent functions. One, $K_{trans} e^{-k_{ep} t}$, can be thought of as a transfer function describing the passage of contrast from the vasculature into the tumor. This transfer function is convoluted with Cp(t) which describes the concentration of contrast in plasma, referred to in the literature as the arterial input function (AIF).

The original Tofts model defines a particular AIF according to the following equation:

$$c_p(t) = a_1 e^{-\mu_1 t} + a_2 e^{-\mu_2 t} \quad (4)$$

Parsing the bi-exponential decay in equation (4) yields that – according to the Tofts model as diagrammed in Figure 1 – the concentration of plasma contrast is governed by a term representing the movement of contrast out of plasma and into

tissue, as well as a second term which governs the slow dissipation of contrast via renal excretion. By substituting equation (4) into equation (3) and holding all parameters as fixed but K_{trans} and v_{e}, different families of curves can be generated as demonstrated in Figure 3. Empirically, one can appreciate that as K_{trans} increases a tumor's curve morphology generally shifts from a continuous uptake curve to a plateau curve to a washout curve. Likewise, as v_{e} increases (i.e. as the cellularity of the tumor decreases), the curves progress from a washout morphology to a continuous uptake morphology.

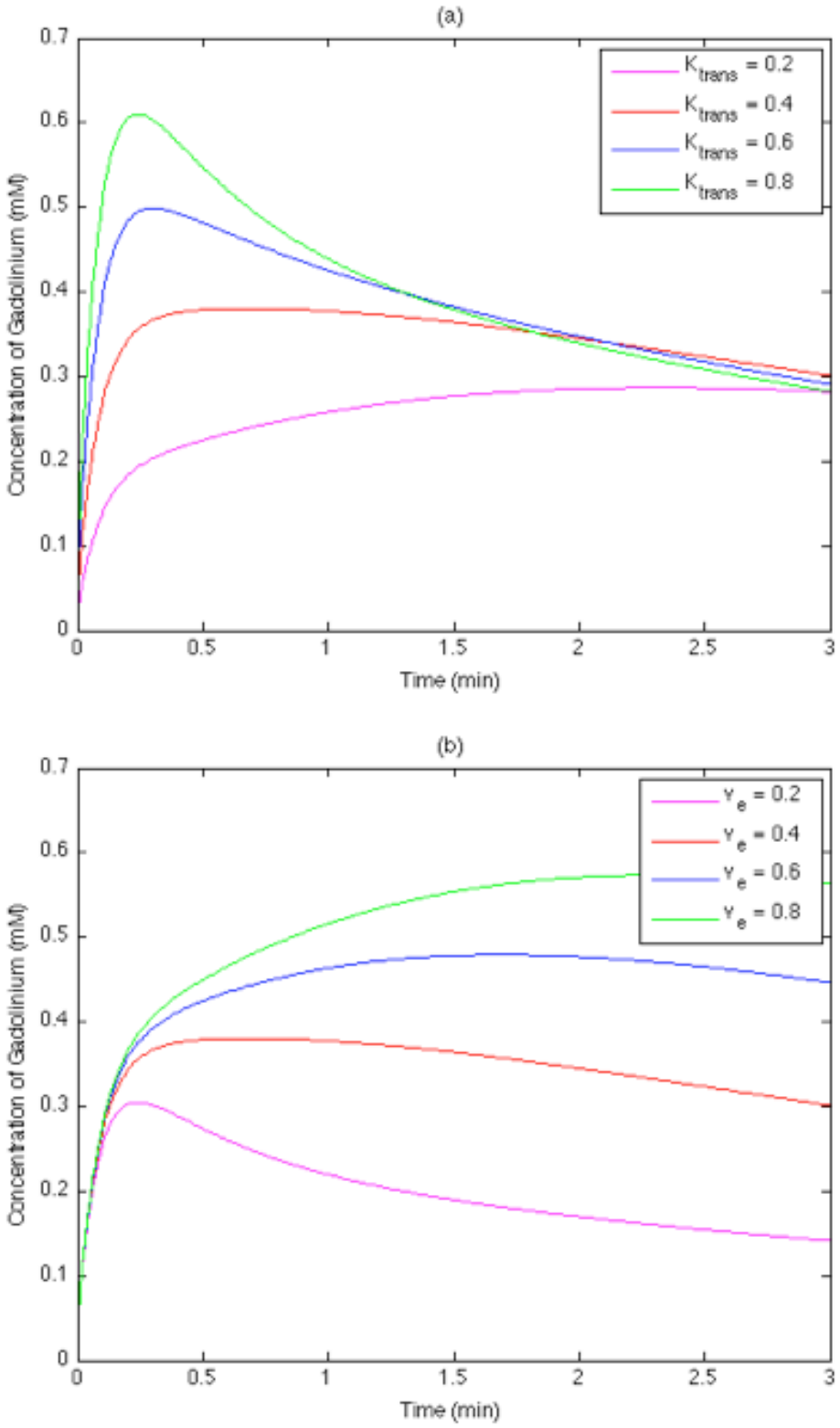

Figure 3 Simulated traces of concentration of gadolinium generated by holding all variables defined in the Tofts model constant and varying only (a) Ktrans and then (b) Ve.

A modification of the standard Tofts model introduces an additional term to account for the fraction of tumor that is occupied by blood vessels. Contrast within microscopic intra-tumoral blood vessels technically contributes to the concentration of contrast within the tumor. This modification, called the extended Tofts model, adds a term to Equation (3) as below

$$c_t(t) = v_p c_p(t) + c_p(t) \otimes \{K_{trans} e^{-k_{ep} t}\} \quad (5)$$

where v_p is the fraction of tumor occupied by blood vessels.

Note additionally that the Tofts AIF represents an idealization of the concentration of contrast in plasma. To be specific, its mathematical form implies that the bolus mixes with the entire plasma volume instantaneously at the same moment of its sudden arrival at the modeled tissue. As seen in Figure 4, the concentration curve begins at a non zero value at t=0, which is non-physiologic. Instead, the vascular mixing of contrast is a complex, stochastic process that takes a finite amount of time. and results in a curve much different from its ideal form in the Tofts AIF. Therefore, for this thesis, we utilized an AIF [$c_p(t)$] based on a measured population input function from the literature. Blood plasma contrast concentration curves were measured in multiple patients and averaged to form a population based AIF which is described by the following empirical equation developed by by Orton et. al.[32]

$$c_p(t) = \begin{cases} a_B(1 - \cos(\mu_B t)) + a_B a_G f(t, \mu_G) & \text{for} \quad 0 \le t \le t_B, \\ a_B a_G f(t_B, \mu_G) e^{-\mu_G (t - t_B)} & \text{for} \quad t > t_B \end{cases} \quad (6)$$

Where,

$$f(t,\alpha) = \frac{1 - e^{-t\alpha}}{\alpha} - \frac{\alpha\cos(\mu_B t) + \mu_B \sin(\mu_B t) - \alpha e^{-t\alpha}}{\alpha^2 + \mu_B^2}$$

$$t_B = \frac{2\pi}{\mu_B}$$

The difference in AIF morphology between Orton's proposed AIF and Tofts original formulation is depicted in Figure 4. It is important to note that while the above equation is not based on any particular physiologic model, the curve it describes matches *in-vivo* contrast concentration curves measured in real patients. [33]). Limitations of using a population based input function are revisited later in this manuscript.

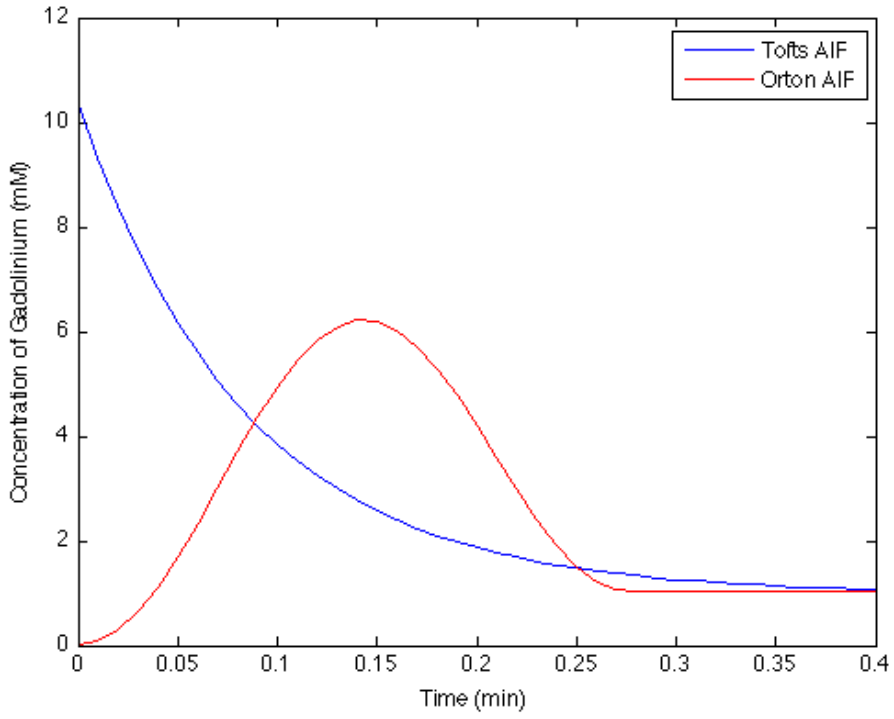

Figure 4 A comparison of the AIFs of both the Tofts model (blue) and that of Orton (red)

Pharmacokinetic Modeling of DCE-MRI and Predicting Patient Response to Neoadjuvant Therapy

K_{trans} is a particularly attractive target for the investigation of potential prognostic biomarkers in the use of anti-angiogensis drugs due to its theoretical association with the vascular barrier in tissue as well as the ability of clinicians to quantify it non-invasively and without ionizing radiation. Unfortunately, the several small studies conducted to date have resulted in inconsistent conclusions and thus, data on the efficacy of PK modeling of DCE-MRI are limited. For instance: Yankeelov et. al. [34] were able to determine a statistically significant shift towards lower K_{trans} in their analysis of populations of voxels from breast lesions undergoing neoadjuvant therapy before and after said therapy. Importantly, while there appeared to be a shift in K_{trans} due to the use of neoadjuvant therapy, responders were not confidently segregated from non-responders and the prognostic value of this observation was left undetermined. Thukral et. al.[35] observed a similar significant shift in the K_{trans} of the voxel populations, but, when compared to pathology data, were unable to show any difference between responders and non-responders. Interestingly, this stands in stark contrast to others such as Ah-See et. al. [36] who were able to differentiate between responders and non-responders by utilizing percentage change in the median value of K_{trans} from baseline. Compounding this confusion of results is the relatively small number of patients this method has been applied to.

This project will attempt to help elucidate this relationship by focusing on prospectively analyzing a group of breast cancer patients according to cutoffs established by several investigators. In 2006 Padhani et. al. [37] noted that an increase, no change, or decrease of less than 11% in the range of K_{trans} calculated over a population of lesion voxels after one cycle of neoadjuvant chemotherapy had an 80% sensitivity and 76% specificity in distinguishing non-responders from responders. Yu et. al.[38] noted by ROC analysis that after two cycles of neoadjuvant chemotherapy, a patient's pathologic response could be predicted (sensitivity 81%, specificity 88%) by calculating the median K_{trans} and using a threshold of percentage change from baseline of -85%. Ah-See et. al. were able to generate a similar threshold after two cycles neoadjuvant chemotherapy for difference in median K_{trans} of -42.1%, however their means of producing this criterion was novel. Before initiating neoadjuvant chemotherapy, Ah-See et. al. performed two baseline imaging studies that could be used to generate a 95% confidence interval for repeatability of the difference in median value of K_{trans}. They then generated the cutoff used in their criterion by utilizing the lower bound of the calculated repeatability interval (i.e. any lower difference could represent a statistically significant effect). With this in mind, this project will not only evaluate the efficacy of each of the mentioned criteria by applying them prospectively, but will also attempt to produce a similar repeatability interval with only a single baseline imaging study. .

Specified Aims

This study aims to better qualify the relationship between the change from baseline of the DCE-MRI measured pharmacokinetic parameter K_{trans}, and a patient's response to neoadjuvant chemotherapy with an anti-angiogenic agent for breast cancer. To accomplish this goal, this project will prospectively apply the cut-offs of change in K_{trans} reported by Padhani et. al., Yu et. al., and Ah-See et. al. to patients undergoing neoadjuvant chemotherapy for breast cancer. Additionally, it will evaluate the efficacy of using a repeatability interval cutoff as described by Ah-See et. al., but generated with only a single baseline imaging study.

Methods

This thesis project was conducted utilizing data acquired as part of an ongoing collaboration between the Yale University School of Medicine (YSM) and the Brown University Oncology Group (BrUOG) to evaluate the effectiveness of neoadjuvant therapy in the treatment of breast cancer. As such, a full description of the methods utilized in this study must necessarily include both the procedures specifically derived to meet the specified aim as well as those developed for the larger collaborative effort, and generative of the data pertinent to this study. To make this distinction explicit, note that the ensuing subsections describing patient recruitment, treatment, and data acquisition are the product of the protocol for the larger collaboration and are were not developed as part of this thesis. Subsections outlining the methods for data and statistical analysis were specifically developed for this thesis.

Patient Recruitment and Treatment

Patients eligible for the larger collaborative effort between YSM and BrUOG were patients with biopsy proven breast cancers larger than 2 cm in size. The collaborative effort attempted to recruit 60 patients with HER2 negative breast cancers and 60 patients with HER2 positive breast cancers. Once admitted, patients were randomized to one of two study arms: one providing traditional, small-

molecule neoadjuvant chemotherapy with paclitaxel and carboplatin, the other utilizing anti-angiogenesis agents (bevacizumab for HER2 negative cancers and trastuzumab for HER2 positive cancers). Before initiating neoadjuvant therapy, a baseline breast MR was obtained. This initial imaging was repeated at +1 week after initiation of neoadjuvant therapy and again at no less than +15 weeks from therapy initiation and prior to planned surgical procedure for removal of the lesion. Surgical specimens were collected at removal for assessment of pathological response. This response was classified into one of three categories: complete response, partial response, and poor response.

To be included in the analysis conducted for this thesis project, patients must have been randomized to the anti-angiogenesis arm of the collaborative study and have been recruited early enough that the previously described baseline and +1 week imaging (hereafter referred to as imaging conducted at time points one and two, respectively) could be obtained, and additionally, have remained in the study long enough that definitive pathological assessment had been conducted and could be included in analysis. Furthermore, each imaging study conducted at time points one and two must have had sufficient temporal resolution to be compatible with PK analysis. A brief description and comparison of the two methods for imaging utilized in the collaborative study ensues.

Data Acquisition

All DCE-MRI studies acquired as part of the collaborative effort were conducted according to one of two methods. The most common sequence (acquired at Brown and at out-patient imaging centers) was designed to produce studies amenable to analysis by the previously mentioned SER method. As such, three volumes were acquired: one prior to administration of gadolinium, one "peak" volume taken at the presumed arrival of bolus (typically 75 seconds post gadolinium administration), and one volume post-arterial phase of contrast (typically at six minutes post-gadolinium). Images were obtained using a 3 dimensional spoiled gradient echo T1 weighted fat suppressed sequence. The resulting studies were of high spatial resolution (2mm x 1 mm x 1mm) and signal to noise, but with only three data points over six minutes – of insufficient temporal resolution to curve-fit the concentration of gadolinium.

The protocol utilized to achieve high temporal resolution utilized an innovative k-space sharing technique (TWIST, Siemens Medical Systems) where the central portions of k-space are oversampled at high temporal resolution and combined with peripheral k-space data acquired at different times. Since contrast information is located in the central k-space regions overall tumor signal intensities are updated at high temporal resolution. Since edge data is contained in the periphery of k-space, which is relatively under-sampled with this technique, tumor margins become slightly less distinct. The details of this technique are beyond the scope of this

thesis. The imaging protocol was determined by the radiologist on the study and was set prior to the initiation of this thesis project.

Images obtained on patients recruited at Yale were obtained using this technique resulting in a high temporal resolution (4-7 seconds per volume) and relatively low spatial resolution (5mm x 1mm x 1 mm) dynamic series using the following parameters: TR: 3.5 ms, TE: 1.5 ms, field of view: 350 mm, and image matrix 320 x 320. For the purposes of T1 mapping (as described subsequently) a reference image was acquired using a flip angle of 3 or 5 degrees. Subsequently, repeated measures were acquired for 5 minutes using a flip angle of 25 degrees. 0.1 mmol / kg of Magnevist IV contrast was injected at 2 cc /sec through an upper extremity peripheral IV after the 4^{th} acquired volume.

Of 30 patients recruited a the Yale site, only 11 were enrolled before their initial MRI and underwent high temporal resolution DCE-MRI before and after initial exposure to chemotherapy. Of these 11 patients, only 7 underwent successful DCE-MRI at both time points. This results in a study population of only 7 patients.

Data Post-Processing

Data gathered as described above were analyzed utilizing a specially developed software platform, DCLab, written by the author in MATLAB. This analysis constituted the central portion of this thesis. One of the primary goals in developing

this software was to allow for the exploration and development of novel and literature proposed pharmacokinetic models in disparate organ systems. As such, DCLab was written according to object-oriented principles to afford modularity and easy extensibility. A brief explanation of the class hierarchy used for the implementation of pharmacokinetic models is outlined in Appendix A. Note that the flexibility afforded authors coding for DCLab is derived from the abstraction and compartmentalization of the various steps in its analytical workflow. A brief overview of that process follows:

1. All images from both dynamic and reference series are loaded into working memory and subsequently organized into discrete, time-sorted collections of volumes
2. The spatial location of a lesion is identified in the dynamic series and the perimeter of an encompassing volume of interest is drawn at the volume's intersection with the acquired slices, thus defining a volume of interest (VOI)
3. An initial (pre-contrast) T1 value for each voxel of the VOI is calculated and stored.
4. Using the baseline T1 values calculated in step 3, the concentration of contrast at each voxel of the VOI over the span of the dynamic series is calculated
5. Each time vs contrast curve generated by step 4 is used to fit a user-selected pharmacokinetic model (in the case of this project, the extended Tofts model with the Orton AIF). The results of which are presented to the user

The ensuing discussion will describe the implementation of pertinent, non-trivial aspects of DCLab's analytical workflow.

Determining Tissue Gadolinium Concentration

Generally in DCE-MRI, converting from measured signal intensity to tissue gadolinium concentration is achieved via one of two separate means. One is the physical construction and use of an apparatus that houses multiple phantoms of known T1 (representing discrete intervals of the full range of T1 expected of gadolinium) that can be placed comfortably alongside the patient[39]. This method ensures both patient and materials of known T1 can be scanned at the same time, therefore allowing T1 to be derived by interpolating the measured signal against a reference curve. However, this is impractical in the setting of a clinical trial performed in a clinical environment. Additionally, there is no room for such a phantom in the breast coils used at our institution.

The second method involves establishing a baseline T1 map of each voxel in the volume of interest (VOI). Measured signal intensity within a VOI is determined by the T1 properties of the tissues within that VOI. As discussed in the following section, the relationship between T1 and measured signal intensity can be determined if the parameters of the imaging sequence are known. Gadolinium concentrations within a given tissue can be determined by first converting changes

in tissue signal intensity to changes in tissue T1. Changes in tissue T1 are related to changes in gadolinium concentration according to the equation delta(Concentration) = 1/Relaxivity(delta1/T1) . Therefore, by measuring how T1 changes within a VOI, one can determine the gadolinium concentration within that VOI.

Calculating a Baseline T1 Map:

According to the Bloch equations, signal S derived from a gradient recalled echo (GRE) sequence with flip angle θ can is represented mathematically as

$$S = M_0 \frac{(1 - E_1)\sin\theta}{1 - E_1 E_2 - (E_1 - E_2)\cos\theta} \tag{7}$$

where $E_1 = e^{-TR/T_1}$, $E_2 = e^{-TR/T_{2*}}$ and M_0 represents the contribution to signal from machine gain, proton density, and T2*. As first observed by Mansfield and Morris [40] when $TR >> T_{2*}$ equation (7) reduces to

$$S = M_0 \frac{(1 - E_1)\sin\theta}{1 - E_1\cos\theta} \tag{8}$$

Rearranging equation (8) produces

$$\frac{S}{\sin\theta} = E_1 \frac{S}{\tan\theta} + M_0(1 - E_1) \tag{9}$$

The key observation that enables calculation of T1 is that equation (9) has the form $Y = mX + b$ where

$$m = E_1$$
$$Y = \frac{S}{\sin\theta}$$
$$X = \frac{S}{\tan\theta}$$

Thus, with two measured signal intensities, S, at the same point spatially but at differentflip angles θ, an initial T1 map can be calculated over the VOI by solving for m at each voxel (E1 contains the constants TR and T1. TR is known and T1 can then be determined). This relationship has been found to be experimentally valid over the expected physiologic range of gadolinium provided that sequence parameters are carefully chosen[41].

One important consideration to facilitating an accurate estimation of local T1 is to correctly select signal to be utilized in the preceding calculations. DCLab accomplishes this by first averaging the signal obtained from each voxel in the VOI over all volumes in the reference series and doing the same for all volumes in the dynamic series that are captured before the local arrival of the contrast bolus. Note that this necessarily requires identifying the time point at which the bolus arrives before any attempts at deriving T1. This is accomplished by expanding the free parameters of the extended Tofts model to fit an additional parameter representing the arrival of the bolus, t_0, as follows:

$$c_t(t) = v_p c_p(t - t_0) + c_p(t - t_0) \otimes \{K_{trans} e^{-k_{ep} t_0}\} \quad (10)$$

It should be noted, however, that the initial T1 map must be estimated before calculation of gadolinium contrast can be accomplished. Because the model

presented in equation (10) is designed for output data in units of concentration of contrast, an approximation must be made at this stage to ensure that any t_0 discovered by matching an objective function based on equation (10) to signal of arbitrary units is accurate. DCLab makes use of a relationship observed by Walker-Samuel et. al.[42] to accomplish this. This relationship holds that, as a reasonable approximation, the concentration of gadolinium in tissue varies linearly over its physiologic range with the following ratio of signals

$$c_t(t) \approx \frac{S(t) - S(0)}{S_r}$$

Where S represents the signal from the dynamic series, and S_r a separate series with a flip angle θ_r such that $\sin\theta_r \approx 0$. In the case of the index imaging study, this criteria is met by the reference series (flip of 3-5 degrees). DCLab thus calculates the average signal ratio over the VOI for each time point in the dynamic series, scales the resulting set to the physiologic range of gadolinium contrast and fits to that set, the model represented by equation (10). In so doing, t_0 can be calculated and the dynamic series segmented into signal obtained before and after bolus arrival.

Calculating the Contrast of Gadolinium

Once the initial T1 map has been calculated, the remaining unknowns in equation (8) can be solved for at time points before the arrival of contrast. In particular, M_0 can be calculated as follows:

$$M_0 = S_\mathrm{d} \frac{1 - E_1 \cos\theta_\mathrm{d}}{(1 - E_1)\sin\theta_\mathrm{d}}$$

Where S_d and θ_d are the signal and flip angle, respectively, of the dynamic series. Because M_0 is not expected to vary with the arrival of gadolinium, the T1 for all voxels in the VOI and at each time point in the dynamic series can be calculated by rearranging equation (8) so that

$$E_1 = \frac{S_\mathrm{d} / M_0 - \sin\theta_\mathrm{d}}{S_\mathrm{d} / M_0 \cos\theta_\mathrm{d} - \sin\theta_\mathrm{d}}$$

Using this equation, the T1 at each time point for all voxels can be calculated, and the concentration of contrast is

$$c_\mathrm{t}(t) = \frac{1}{R_{1,\mathrm{gad}}} \left(\frac{1}{T_1(t)} - \frac{1}{T_1(0)} \right)$$

Where $R_{1,\mathrm{gad}}$ is the unit longitudinal relaxivity of Magnevist in plasma.

Fitting the Extended Tofts Model

The mechanics of matching the extended Tofts model defined in equation (5) to the observational data requires special explanation. DCLab utilizes the Levenberg-Marquardt non-linear least squares curve-fitting algorithm as it has been shown to generate superior performance with regard to percentage of data accurately fit than other employed methods[43]. The Levenberg-Marquardt algorithm searches through an N-d problem space, where N is the number of parameters to be fit, by iteratively

perturbing each of the target parameters so as to minimize the sum-squared error of an objective function (in this case, the extended Tofts model) to provided observational data. Like all optimization algorithms of this sort, the performance of Levenberg-Marquardt is seed-dependent: its ultimate output may represent a local, rather than global, minimum in the problem space.

DCLab attempts to reduce this potential for error by allowing a user to seed Levenberg-Marquardt with an arbitrary number of "initial guesses" and returning the parameters that resulted in the single "best." Note that, in this study, the number of guesses chosen represents a compromise between compute time and coverage of the problem space. To be specific, the problem space spanned by physiologic K_{trans} and v_{e} (note that v_{p} was not included as its physiologic range is much smaller than either of the other two utilized parameters) was divided into 4 equally sized segments, the centers of which were each included as an initial seed. In addition, the center of the entire previously-described problem space and the parameters that generated the last successful fit were also included. Using this set of seeds the Levenberg-Marquardt algorithm was run for each time vs. concentration trace at each voxel in the VOI. A "successful fit" was defined as algorithmic output that yielded parameters falling within their known physiologic range (for instance v_{e} and v_{p} are fractions ranging from 0 to 1, an algorithmic output yielding a value for either above 1 or beneath 0 was rejected). If more than one seed was successfully fit, the set of output parameters that yielded the lowest sum-squared error was chosen

as the returned fit for each voxel. If no seed was successfully fit, the voxel was removed from further analysis.

Fixed PK Parameter Valuation

As noted previously, DCLab utilizes a population-based AIF. The fixed parameters noted in Equation (6) are provided by Orton[32] and were produced via modeling on simulated data[44]. Additionally, the unit longitudinal relaxivity of Magnevist in plasma was obtained from in-vivo estimations reported by Pintaske et. al. [45].

Statistical Analysis

All patient studies processed by DCLab had the following measurements recorded: the median and range of K_{trans} over all voxels in the VOI and a histogram of the K_{trans} calculated at each voxel in the VOI. A non-parametric Mann-Whitney U test was utilized to compare the percentage change in median K_{trans} from time point one to two between responders and non-responders by pathology. Percentage change in median K_{trans} was compared to cutoffs of an increase, no change, or less than 85% (in the case of the Yu criterion) and 42% (in the case of the Ah-See criterion) decrease in K_{trans} to classify each patient meeting the criterion as a "predicted non-responder" otherwise a "predicted responder". Similarly, a percentage change of the range of K_{trans} that showed an increase, no change, or less than 11% decrease was classified as a "predicted non-responder" and otherwise a "predicted responder."

This thesis additionally calculated a repeatability range for the difference in median K_{trans}, the lower bound of which was utilized as an additional criterion for predicting pathologic response. Because this thesis had imaging from only a single study before the administration of neoadjuvant chemotherapy, the repeatability range could not be calculated by strictly repeating Ah-See's method. Instead, it was found by first randomly segmenting the baseline lesion voxels into two distinct populations for each patient. Using these two populations the difference median K_{trans} could be calculated and, according to Ah-See, the repeatability range is

$$\pm 1.96\sqrt{\sum d^2 / n}$$

Where *n* is the number of studies and *d* is the percentage change in median K_{trans}. Thus, if the percentage change showed an increase, no change, or decrease less than that provided by the lower bound of the repeatability range it was classified a "predicted non-responder," otherwise a "predicted responder."

Results

To date, 106 women have been admitted to the anti-angiogenic arm of the YSM/BrUOG trial. 30 of this cohort have undergone the high-temporal DCE-MRI. However, since most of the patients were enrolled after an initial clinical breast MRI detected their breast cancer, only 11 patients had high temporal resolution DCR-MRI performed at baseline. Of these, four had to be dropped from analysis due to incorrectly acquired reference series (n=2), unrecorded reference series (n=1), or a dynamic series with image acquisition begun post-bolus arrival (n=1).

On analysis of the surgical specimens acquired after completion of neoadjuvant chemotherapy, two women were noted to have lesions that responded by pathology and five were classified non-responders.

The calculation of K_{trans} over all voxels of each included patient's lesion can be described via the statistical descriptors reported in Table (1) and representative histograms detailing the transformation of K_{trans} from time point one to two are diagrammed in Figure (5) for representative patients. In addition, the average concentration of contrast over lesions taken from time points one and two – as well as their best-fit model-generated curve – are provided from the same patients in Figure (6).

Patient ID	Time Point	Percent Fit	Mean K_{trans}	Median K_{trans}	Range K_{trans}	Pathological Response
1	1	63%	0.107±0.06	0.096	0.717	Negative
	2	78%	0.212±0.13	0.174	0.867	
2	1	60%	0.516±0.24	0.514	1.678	Negative
	2	55%	0.470±0.20	0.441	0.981	
3	1	73%	0.500±0.20	0.500	1.408	Negative
	2	40%	0.421±0.22	0.377	1.414	
4	1	96%	0.106±0.05	0.062	0.913	Negative
	2	90%	0.229±0.15	0.204	0.917	
5	1	79%	0.149±0.10	0.137	0.556	Negative
	2	62%	0.202±0.11	0.180	0.647	
6	1	84%	0.358±0.19	0.315	1.168	Positive
	2	82%	0.096±0.03	0.082	0.459	
7	1	73%	0.590±0.24	0.606	0.999	Positive
	2	79%	0.474±0.26	0.432	1.015	

Table 1 For both time points collected for each patient, the percentage of lesion voxels fit via PK modeling; the pathological response of the lesion to antiangiogenic therapy; and statistical descriptors of the Ktrans calculated for each voxel in the target lesion.

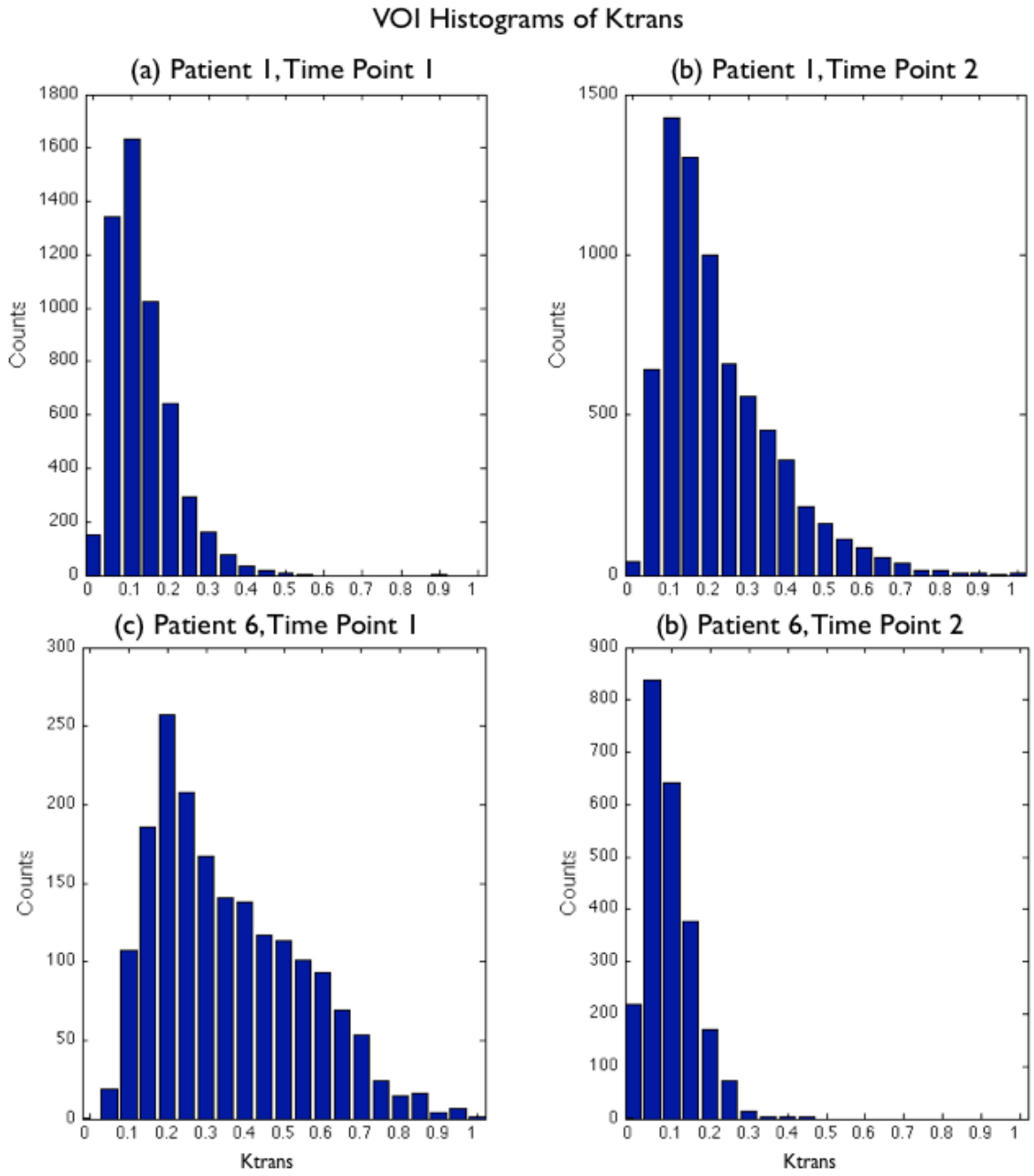

Figure 5 Histograms of the calculated per-voxel Ktrans over a lesion's VOI. Note that patient 1 is a non-responder by pathology; her Ktrans histograms are given at time points (a)1 and (b) 2. Patient 6 is a responder by pathology; her Ktrans histograms are given at time points (a) 1 and (b) 2.

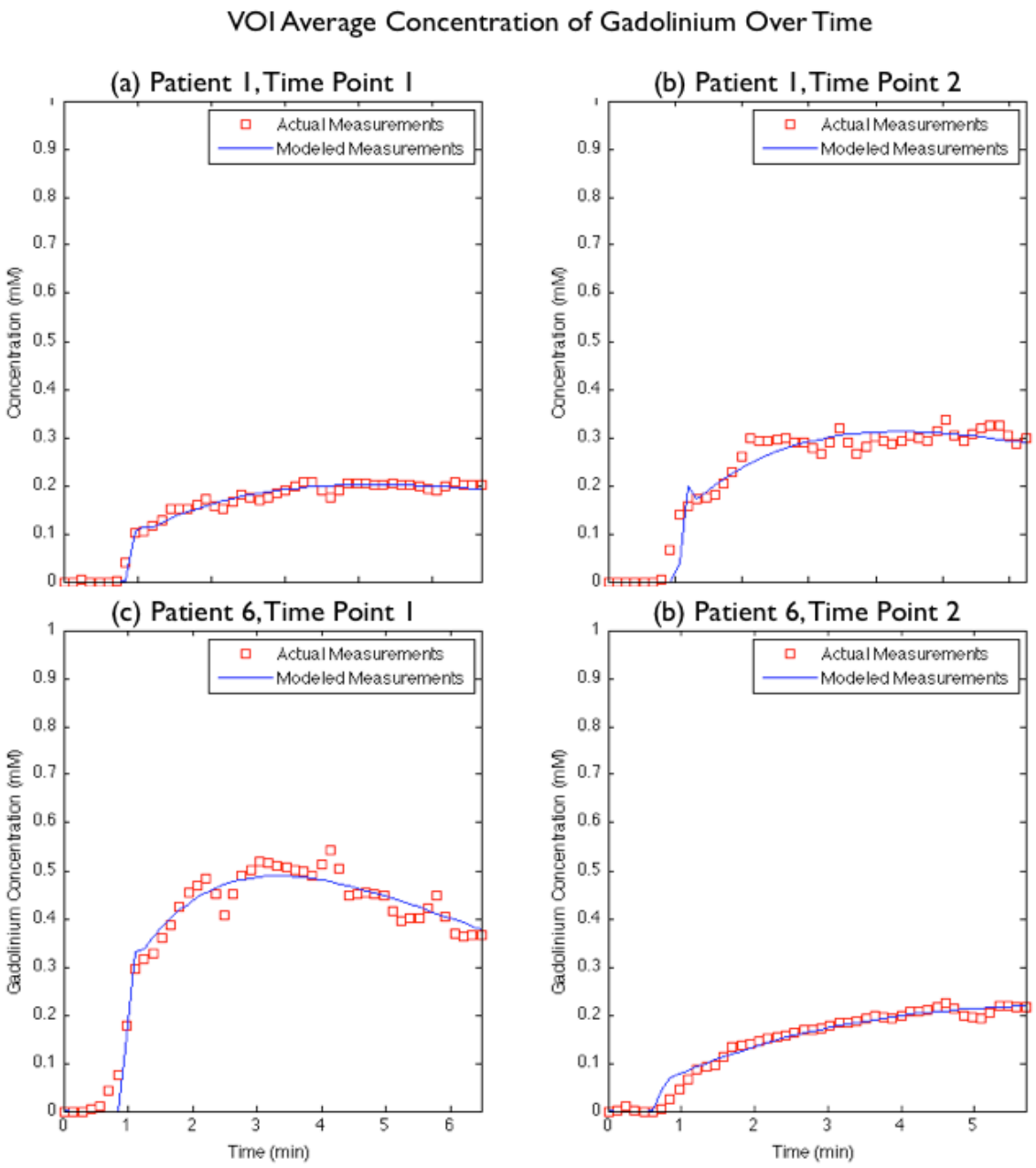

Figure 6. Traces of the average measured concentration of contrast over a lesion's VOI as well as the trace of the best-fit PK model. Note that patient 1 is a non-responder by pathology. (a) Gives her average trace and fit at time point 1 (modeled Ktrans=0.108, Ve=0.325), and (b) her average trace and fit at time point 2 (modeled Ktrans=0.1684, Ve=0.500). Patient 6 is a responder by pathology. (a) Gives her average trace and fit at time point 1 (modeled Ktrans=0.295, Ve=0.694), and (b) her average trace and fit at time point 2 (modeled Ktrans=0.135, Ve=0.565).

By performing the non-parametric Mann-Whitney U test for significance on the difference between median K_{trans} values from time point one to two and using an

$\alpha = 0.05$, the mean difference between the responders and non-responders cannot be determined to be statistically significant at this level of power (p=0.0952).

After scaling the pertinent values in Table (1) against their respective initial levels at time point one, the Padhani, Yu, and Ah-See criteria for identifying pathological responders can be applied. The results of doing so are provided in Table (2) for all criteria.

ID	%Δ Median	%Δ Range	Padhani Criterion %Δ Range < -11%	Yu Criterion %Δ Median < -85%	Ah-See Criterion %Δ Median < -42.1%	%Δ Median < -39.4%	PR
1	+82%	+21%	-	-	-	-	-
2	-14%	-42%	+	-	-	-	-
3	-24%	0%	-	-	-	-	-
4	+116%	0%	-	-	-	-	-
5	+36%	+16%	-	-	-	-	-
6	-73%	-61%	+	-	+	+	+
7	-29%	+2%	-	-	-	-	+

Table 2 Predicted Response to Therapy According to Literature and Proposed Criteria. For each patient in the study (ID), the percentage change between time points one and two of the median and range of Ktrans are provided. Utilizing these values, the results of applying the Padhani, Yu, Ah-See, and the proposed criteria are shown (note that "+" is equivalent to "predicted responder" and "-" is equivalent to "predicted non-responder") as well as the final pathological response (PR).

By running twenty-five simulations where each lesion at time point one was segmented into two distinct populations randomly and their difference in median K_{trans} was utilized to calculate a repeatability interval, the average lower bound was -34.7 ± 3.76%. The result of using this criterion to predict pathological response by individual patients is provided in Table (2).

Discussion

Although the limited amount of data associated with this project necessarily limits the conclusions one may draw, there remain several observations that necessitate consideration. This discussion will focus on trends and findings either in agreement with or opposition to previously published work.

Many of the preceding experiments (excepting Padhani) that attempt to derive a means of predicting pathological response to neoadjuvant therapy by way of change over a population of K_{trans} remark that, retrospectively, the difference between median K_{trans} from some point during therapy to baseline is significantly different if a patient is determined to have responded to therapy than if she hasn't. This finding could not be reproduced in this thesis. The reason here is unsatisfying: this study is simply too underpowered. Note that the statistical test for determining a difference between the means of two potentially different datasets, the Mann-Whitney U test, cannot generate a *p* value less than that noted above (p=0.0952) for any member valuation of sets of cardinality 2 and 5. The responders in this study have greater negative difference in median K_{trans} than non-responders: the trend is in the correct direction.

While the absolute values of K_{trans} reported in this thesis appear to fall within the range of that reported elsewhere, one glaring difference deserves consideration. Specifically, previous reports that utilize curve fitting have yielded higher percentages of voxels fit than here. One important point, when considering why this may be, is to focus on the centrality of the shape of the population-derived AIF to the morphologic range of concentration curves that can be fit with physiologically ranged free parameters.

A population-derived AIF is static; it cannot account for variation in the speed at which the bolus was pushed, the patient's cardiac output, nor the process of contrast mixing (among other factors). Consider that by doubling the parameter a_1 in Equation (6), any fit by this new model to a given concentration curve will yield K_{trans} and v_e exactly half of that predicted by the model valuations utilized in this project. Thus, with an AIF that is not a good approximation of plasma contrast, the model fitting stage may generate non-physiologic free parameters that would result in a voxel's rejection (for instance, a "true" a_1 valued half of that utilized here would result in the rejection of all voxels with "true" v_e ranged 0.5-1). This is a limitation intrinsic to utilizing population-derived AIF: individual variation is lost, thus – in addition to lower voxel matching rates if the AIF is not reasonably close to "true"-- accuracy in K_{trans} calculations is reduced.

This potential source of error is accounted for in this study through the use of an automated means for supplying the contrast bolus, and by assuming that a patient's

physiology will not change sufficiently to alter the shape of the bolus between studies. Because this study considers *percentage* change between two time points, it is assumed that any error produced by an incorrect AIF in analysis will be sufficiently reproduced at the second time point as to be negligable. Considering the non-linearity of the Tofts model, this may not be a reasonable assumption. Note that this issue is not addressed in previous studies.

Alternatives to using a population derived AIF are to create a patient specific AIF based on the first pass of contrast through an artery in the imaged field of view. An automated technique for this was first described in 2001[46] and this technique has been used in similar studies performed at the NCI[20]. However, the assumptions used in the T1 mapping scheme described above do not hold at gadolinium concentrations normally found in arterial blood (at high concentrations the signal intensity can saturate due to T2* effects). This was shown in the reference discussed in the next paragraph. Subsequent errors in the AIF would result in the same problems described above.

Another alternative solution is to administer a small bolus of contrast (roughly 10% of the normal dose) and use this bolus to prospectively construct an AIF scaled to a subsequent injection[47]. This technique has not, to our knowledge, been applied in any published studies. Additionally, the authors who describe this technique did not calculate the AIF using T1 mapping techniques. Instead, they assumed that contrast equation scaled linearly with relative signal enhancement (i.e. a doubling in

signal intensity equaled a doubling in concentration) which is not quantatively accurate. It is not clear how this assumption affects the calculated AIF and thus the subsequent calculations.

A third alternative is to utilize a reference method first described by Yankeelov[48]. In this method, time enhancement curves are measured in a non-neoplastic tissue such as pectoralis muscle. Using assumed values of K_{trans} and k_{ep} for these tissues, the Tofts model is solved for the AIF. This AIF is then used for analysis of the tumor enhancement curve. Potential problems with this method mirror those of using a population AIF in that it is not known how constant pectoralis muscle K_{trans} is throughout the population. Additionally, these values may be affected by chemotherapy and change over time. To account for this some authors have modified the technique to report a tumor K_{trans} scaled to that of the reference tissue[49] and perform ROC analyses based on those values. This makes comparing perfusion results from patient to patient and from study to study difficult because the reported parameter is not tumor specific. An additional problem with the reference method is that for this study the physical geometry of the breast coil used in the MRI exam results in decreased signal to noise in the muscles due to their posterior location. Reference imaging is more practical when studying neoplasms like cervical and prostate cancer where reference muscles are located near the center of the field of view.

A second limitation in the computation algorithm is the technique used for T1 mapping. Equation (9) above should produce an accurate calculation of T1 in ideal circumstances. The B1 field must be homogenous throughout the entire field of view, the longitudinal magnetization must be in steady state, and the transverse magnetization must be completely spoiled before each repeated excitation. More sophisticated techniques have been developed that take these potential confounders into consideration[50]. The study scan protocol did not allow for this type of analysis.

Additionally, T1 histogram analysis revealed a large variation in measured T1 values across structures that should be relatively homogenous, such as adipose tissue in the breast (for an example, see Figure 7). This suggests that the pre-contrast reference series, obtained a low flip angle, may have had insufficient signal to noise to be accurately used in the analysis. For this reason, we performed most of our analyses on mean tumor regions of interest as opposed to voxel by voxel analyses. Averaging signal from all the voxels in the tumor resulted in baseline T1 measurements more in line with those in the literature.

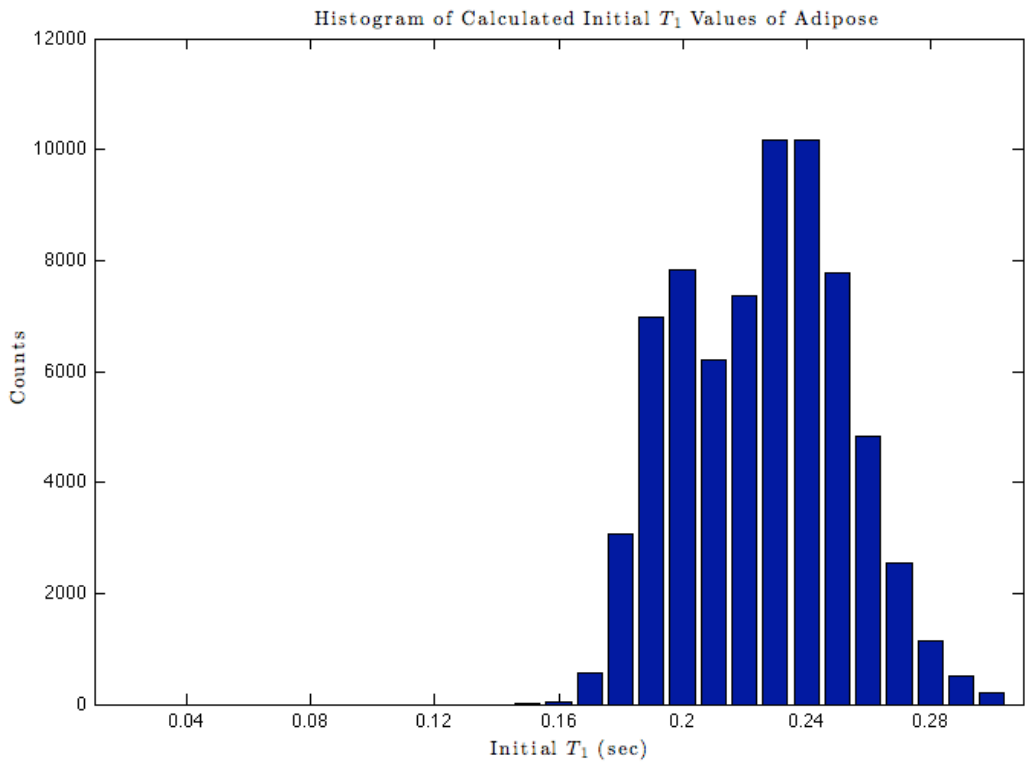

Figure 7 Histogram of calculated initial T1 over all voxels in a volume of interest placed over breast adipose tissue (true adipose T1 is approximately 300ms)

The performance of each criterion used for prediction of response to therapy also necessitates remarks. In particular, the Padhani criterion is extremely difficult to justify. In carefully considering their study design, note that Padhani et. al. rejected all voxels that yielded K_{trans} greater than 0.5/sec because valuation above that cutoff was said to have an unclear physiological meaning. This arbitrary cutoff necessarily sets an upper-bound on the possible K_{trans} range, and thus effects their receiver operating characteristic analysis. Additionally, the AIF they chose for their study is the same as that for the original Tofts model and given in Equation (4). Because the Tofts AIF does not accurately reflect the true concentration of contrast in plasma, the absolute value of the K_{trans} generated via their method may vary with true K_{trans}, but it may not be accurately valued. Thus, their use of a cutoff is highly questionable;

without it, the range trends reported in their results would be much more susceptible to noise.

That the Ah-See and Yu criteria were both able to correctly predict all non-responders while failing to accurately do the same for positive responders is interesting. One possible explanation is that each of their criteria was applied after completion of the second cycle of neoadjuvant chemotherapy. In this thesis, they are applied after the first. Presumably, with more time, the responders could reach the cutoffs reported. Another explanation is simply that neither criterion was reported to have 100% sensitivity. Thus, with our limited data, it is impossible to tell if this failure represents a significant difference.

Finally, the performance of our data-generated cutoff appears promising. By judging the performance of each criterion to how closely it's determinant value is to one that would accurately segment the two populations, ours performed best. That said, had imaging been performed at two cycles instead of one, the accuracy of Ah-See and Yu may have been higher. On the question of the difference between the values of our cutoff and Ah-See's, there are several possible reasons. Specifically, contributions to the repeatability range accounted for by Ah-See's method, but not ours, are imaging parameter inaccuracies, errors of slice selection, and differences in coil placement between studies (among others). Conversely, our data (unlike Ah-See's) were generated with heterogeneous imaging parameters. With both of these important differences in mind, note that Ah-See's cutoff falls within one standard of deviation

of our average value. It is certainly plausible that their value could just as easily have been generated on their data using our method. On examination of Ah-See's paper, it appears possible to separate data with 100% accuracy into three categories: those with change of median K_{trans} below –43.7% (our mean value, minus one standard deviation) as predicted pathological responders, those with change of median K_{trans} above -35.1% (our mean value plus one standard deviation) as predicted pathological non-responders, and those few in-between needing further evaluation. This is all speculative but our results do suggest it is possible to generate a suitable repeatability range by segmentation of a single lesion. More data are needed for any meaningful conclusions.

Considering the results presented here, there are several potential interesting avenues for future research. As patients continue to be enrolled in the Yale/BrUOG study, the analysis begun and described as part of this thesis can be continued to better elucidate the validity of the retrospectively-derived criteria. Additional patients may also influence our measured repeatability range. It should also be noted that DCLab was written to be extended and modified, thus there is potential for its future utilization in research on novel targets and via novel models.

References

1. Ferrara N. Molecular and biological properties of vascular endothelial growth factor. J Mol Med 1999;77(7):527–543.

2. Kim KJ, Li B, Winer J, et al. Inhibition of vascular endothelial growth factor-induced angiogenesis suppresses tumour growth in vivo. Nature 1993;362(6423):841–844.

3. Millauer B, Shawver LK, Plate KH, Risau W, Ullrich A. Glioblastoma growth inhibited in vivo by a dominant-negative Flk-1 mutant. Nature 1994;367(6463):576–579.

4. Cobleigh MA, Langmuir VK, Sledge GW, et al. A phase I/II dose-escalation trial of bevacizumab in previously treated metastatic breast cancer. Semin Oncol 2003;30(5 Suppl 16):117–124.

5. Yang JC, Haworth L, Sherry RM, et al. A randomized trial of bevacizumab, an anti–vascular endothelial growth factor antibody, for metastatic renal cancer. The New England journal of medicine 2003;349(5):427–434.

6. Kabbinavar F, Hurwitz HI, Fehrenbacher L, et al. Phase II, randomized trial comparing bevacizumab plus fluorouracil (FU)/leucovorin (LV) with FU/LV alone in patients with metastatic colorectal cancer. J Clin Oncol 2003;21(1):60–65.

7. Valtola R, Salven P, Heikkilä P, et al. VEGFR-3 and its ligand VEGF-C are associated with angiogenesis in breast cancer. Am J Pathol 1999;154(5):1381–1390.

8. Linderholm B, Grankvist K, Wilking N, Johansson M, Tavelin B, Henriksson R. Correlation of vascular endothelial growth factor content with recurrences, survival, and first relapse site in primary node-positive breast carcinoma after adjuvant treatment. J Clin Oncol 2000;18(7):1423–1431.

9. Gasparini G, Toi M, Gion M, et al. Prognostic significance of vascular endothelial growth factor protein in node-negative breast carcinoma. J Natl Cancer Inst 1997;89(2):139–147.

10. Robert NJ, Dieras V, Glaspy J, et al. RIBBON-1: Randomized, Double-Blind, Placebo-Controlled, Phase III Trial of Chemotherapy With or Without Bevacizumab for First-Line Treatment of Human Epidermal Growth Factor Receptor 2-Negative, Locally Recurrent or Metastatic Breast Cancer. Journal of Clinical Oncology 2011;29(10):1252–1260.

11. Miller K, Wang M, Gralow J, et al. Paclitaxel plus bevacizumab versus paclitaxel alone for metastatic breast cancer. The New England journal of medicine 2007;357(26):2666–2676.

12. Gray R, Bhattacharya S, Bowden C, Miller K, Comis RL. Independent Review of E2100: A Phase III Trial of Bevacizumab Plus Paclitaxel Versus Paclitaxel in Women With Metastatic Breast Cancer. Journal of Clinical Oncology 2009;27(30):4966–4972.

13. World Health Organization. WHO handbook for reporting results of cancer treatment. 1979.

14. Therasse P. New Guidelines to Evaluate the Response to Treatment in Solid Tumors. J Natl Cancer Inst 2000;92(3):205–216.

15. Ellis L. Mechanisms of Action of Bevacizumab as a Component of Therapy for Metastatic Colorectal Cancer 10.1053/j.seminoncol.2006.08.002 : Seminars in Oncology | ScienceDirect.com. Semin Oncol 2006;

16. Fisher B, Bryant J, Wolmark N, et al. Effect of preoperative chemotherapy on the outcome of women with operable breast cancer. J Clin Oncol 1998;16(8):2672–2685.

17. Machiavelli M, Romero A, Pérez J, et al. Prognostic significance of pathological response of primary tumor and metastatic axillary lymph nodes after neoadjuvant chemotherapy for locally advanced breast carcinoma. Cancer J Sci Am 1998;4(2):125–31.

18. O'Connor JPB, Carano RAD, Clamp AR, et al. Quantifying antivascular effects of monoclonal antibodies to vascular endothelial growth factor: insights from imaging. Clin Cancer Res 2009;15(21):6674–6682.

19. Padhani AR, Hayes C, Assersohn L, et al. Prediction of Clinicopathologic Response of Breast Cancer to Primary Chemotherapy at Contrast-enhanced MR Imaging: Initial Clinical Results. Radiology 2006;239(2):361–374.

20. Ocak I, Bernardo M, Metzger G, et al. Dynamic Contrast-Enhanced MRI of Prostate Cancer at 3 T: A Study of Pharmacokinetic Parameters. American Journal of Roentgenology 2007;189(4):W192–W201.

21. Sourbron S, Ingrisch M, Siefert A, Reiser M, Herrmann K. Quantification of cerebral blood flow, cerebral blood volume, and blood-brain-barrier leakage with DCE-MRI. Magnetic Resonance in Medicine 2009;62(1):205–217.

22. Jarnagin WR, Schwartz LH, Gultekin DH, et al. Regional chemotherapy for unresectable primary liver cancer: results of a phase II clinical trial and assessment of DCE-MRI as a biomarker of survival. Ann Oncol

2009;20(9):1589–1595.

23. Zahra MA, Tan LT, Priest AN, et al. Semiquantitative and quantitative dynamic contrast-enhanced magnetic resonance imaging measurements predict radiation response in cervix cancer. Int J Radiat Oncol Biol Phys 2009;74(3):766–773.

24. Kuhl C, Mielcareck P, Klaschik S, Leutner C. Dynamic Breast MR Imaging: Are Signal Intensity Time Course Data Useful for Differential Diagnosis of Enhancing Lesions?1. Radiology 1999;

25. Schnall M, Blume J, Bluemke D. Diagnostic Architectural and Dynamic Features at Breast MR Imaging: Multicenter Study1. Radiology 2006;

26. Khouli El RH, Macura KJ, Jacobs MA, et al. Dynamic Contrast-Enhanced MRI of the Breast: Quantitative Method for Kinetic Curve Type Assessment. American Journal of Roentgenology 2009;193(4):W295–W300.

27. Buadu L, Murakami J, Murayama S. Breast lesions: correlation of contrast medium enhancement patterns on MR images with histopathologic findings and tumor angiogenesis. Radiology 1996;

28. Medved M, Karczmar G, Yang C, et al. Semiquantitative analysis of dynamic contrast enhanced MRI in cancer patients: Variability and changes in tumor tissue over time. J Magn Reson Imaging 2004;20(1):122–128.

29. Li K-L, Henry RG, Wilmes LJ, et al. Kinetic assessment of breast tumors using high spatial resolution signal enhancement ratio (SER) imaging. Magnetic Resonance in Medicine 2007;58(3):572–581.

30. Li KL, Partridge SC, Joe BN, et al. Invasive Breast Cancer: Predicting Disease Recurrence by Using High-Spatial-Resolution Signal Enhancement Ratio Imaging. Radiology 2008;248(1):79–87.

31. Leach MO, Brindle KM, Evelhoch JL, et al. The assessment of antiangiogenic and antivascular therapies in early-stage clinical trials using magnetic resonance imaging: issues and recommendations. Br. J. Cancer. 2005;92(9):1599–1610.

32. Orton MR, d'Arcy JA, Walker-Samuel S, et al. Computationally efficient vascular input function models for quantitative kinetic modelling using DCE-MRI. Physics in Medicine and Biology 2008;53(5):1225–1239.

33. Woolrich MW, Jenkinson M, Brady JM, Smith SM. Fully Bayesian Spatio-Temporal Modeling of FMRI Data. Medical Imaging, IEEE Transactions on 2004;23(2):213–231.

34. Yankeelov TE, Lepage M, Chakravarthy A, et al. Integration of quantitative DCE-MRI and ADC mapping to monitor treatment response in human breast cancer: initial results. Magn Reson Imaging 2007;25(1):1–13.

35. Thukral A, Thomasson D, Chow C, Eulate R. Inflammatory Breast Cancer: Dynamic Contrast-enhanced MR in Patients Receiving Bevacizumab—Initial Experience1. Radiology 2007;

36. Ah-See MLW, Makris A, Taylor NJ, et al. Early Changes in Functional Dynamic Magnetic Resonance Imaging Predict for Pathologic Response to Neoadjuvant Chemotherapy in Primary Breast Cancer. Clinical Cancer Research 2008;14(20):6580–6589.

37. Padhani AR, Hayes C, Assersohn L, et al. Prediction of Clinicopathologic Response of Breast Cancer to Primary Chemotherapy at Contrast-enhanced MR Imaging: Initial Clinical Results. Radiology 2006;239(2):361–374.

38. Yu Y, Jiang Q, Miao Y, et al. Quantitative Analysis of Clinical Dynamic Contrast-enhanced MR Imaging for Evaluating Treatment Response in Human Breast Cancer. Radiology 2010;257(1):47–55.

39. d'Arcy JA, Collins DJ, Rowland IJ, Padhani AR, Leach MO. Applications of sliding window reconstruction with cartesian sampling for dynamic contrast enhanced MRI. NMR Biomed 2002;15(2):174–183.

40. Mansfield P. Mansfield and Morris (1982) NMR imaging in biomedicine. 1982.

41. Schabel MC, Parker DL. Uncertainty and bias in contrast concentration measurements using spoiled gradient echo pulse sequences. Physics in Medicine and Biology 2008;53(9):2345–2373.

42. Walker-Samuel S, Leach M, Collins D. Reference tissue quantification of DCE-MRI data without a contrast agent calibration. Physics in Medicine and Biology 2007;52:589.

43. Ahearn TS, Staff RT, Redpath TW, Semple SIK. The use of the Levenberg-Marquardt curve-fitting algorithm in pharmacokinetic modelling of DCE-MRI data. Physics in Medicine and Biology 2005;50(9):N85–92.

44. Parker GJM, Roberts C, Macdonald A, et al. Experimentally-derived functional form for a population-averaged high-temporal-resolution arterial input function for dynamic contrast-enhanced MRI. Magn Reson Med 2006;56(5):993–1000.

45. Pintaske J, Martirosian P, Graf H, Erb G. Relaxivity of gadopentetate dimeglumine (Magnevist), gadobutrol (Gadovist), and gadobenate dimeglumine (MultiHance) in human blood plasma at 0.2, 1.5, and 3 ….

Investigative … 2006;

46. Rijpkema M, Kaanders JH, Joosten FB, van der Kogel AJ, Heerschap A. Method for quantitative mapping of dynamic MRI contrast agent uptake in human tumors. J Magn Reson Imaging 2001;14(4):457–463.

47. Makkat S, Luypaert R, Sourbron S, Stadnik T, De Mey J. Assessment of tumor blood flow in breast tumors with T1-dynamic contrast-enhanced MR Imaging: Impact of dose reduction and the use of a prebolus technique on diagnostic efficacy. Journal of Magnetic Resonance Imaging 2010;31(3):556–561.

48. Yankeelov TE, Luci JJ, Lepage M, et al. Quantitative pharmacokinetic analysis of DCE-MRI data without an arterial input function: a reference region model. Magn Reson Imaging 2005;23(4):519–529.

49. Haider MA, Sitartchouk I, Roberts TPL, Fyles A, Hashmi AT, Milosevic M. Correlations between dynamic contrast-enhanced magnetic resonance imaging–derived measures of tumor microvasculature and interstitial fluid pressure in patients with cervical cancer. J Magn Reson Imaging 2007;25(1):153–159.

50. Treier R, Steingoetter A, Fried M, Schwizer W, Boesiger P. Optimized and combined T1 and B1 mapping technique for fast and accurate T1 quantification in contrast-enhanced abdominal MRI. Magnetic Resonance in Medicine 2007;57(3):568–576.